# MATERIAL DESIGN OF III-NITRIDE TERNARY VIA FIRST PRINCIPLES CALCULATIONS

**ROBIN CHANG YEE HUI**

**UNIVERSITI SAINS MALAYSIA**

**2017**

# MATERIAL DESIGN OF III-NITRIDE TERNARY VIA FIRST PRINCIPLES CALCULATIONS

**by**

**ROBIN CHANG YEE HUI**

**Thesis submitted in fulfillment of the requirements**
**for the degree of**
**Doctor of Philosophy**

**October 2017**

## ACKNOWLEDGEMENT

First and foremost, I would like to express my profound gratitude and appreciation to Dr Yoon Tiem Leong, my project supervisor, for the constant guidance and inspiration. On a personal level, I always feel that his non-pushy and easy-going styles are the qualities that make him very approachable. Many of us would have frequent meal cum discussion sessions with him.

Sincere thanks also goes to Dr Lim Thong Leng for taking me under his wings throughout my study. I will never forget how the first meeting with him at Oldtown White Coffee Melaka has helped me in gaining the required breakthrough. The meeting was so fruitful, making the seven hours road trip an extremely worthy one.

Having the chance to work with terrific personnel like Goh Eong Sheng, Mah Jian Wen, Koh Pin Wai, Timothy Tie to name a few, made my researching work even more enjoyable and rewarding. I have grasped a great deal about condensed matter physics during that period, largely due to their willingness to teach and company. Thank you, my friends. I look forward to a long-lasting friendship among us.

To my wife and energy source, Sharon Tuh, I cannot thank you enough for the unwavering encouragement and support. You are always there for me through thick and thin. Life without you is something I dare not imagine.

## TABLE OF CONTENTS

## LIST OF TABLES

## LIST OF FIGURES

## LIST OF ABBREVIATIONS

| | |
|---|---|
| **DFT** | Density functional theory |
| **DFPT** | Density functional perturbation theory |
| **USPEX** | Universal Structure Predictor: Evolutionary Xtallography |
| **LDA** | local density approximation |
| **GGA** | generalized gradient approximation |
| ***GW*** | Green's function and screened Coulomb interaction |
| **RPA** | Random Phase Approximation |
| **EM** | electromagnetic |
| **BoltzTraP** | Boltzmann Transport |
| **VASP** | Vienna Ab initio Simulation Package |
| **BZ** | Brillouin zone |
| **IBZ** | Irreducible Brillouin zone |
| ***ZT*** | figure of merit |
| **VBM** | valence band maximum |
| **CBM** | conduction band minimum |
| **SHG** | second harmonic generation |

## LIST OF SYMBOLS

| | |
|---|---|
| $E_g$ | energy band gap |
| $H$ | Hamiltonian |
| $\varphi$ | wavefunction |
| $n(\boldsymbol{r})$ | charge density |
| $V(\boldsymbol{r})$ | potential |
| $C_{xy}^{\alpha\beta}(\boldsymbol{q})$ | dynamical matrix |
| $C_{ij}$ | elastic coefficient |
| $e_{ij}$ | piezoelectric coefficient |
| $P$ | polarization |
| $\varepsilon$ | dielectric constant |
| $\beta$ | skew angle |
| $\theta_D$ | Debye temperature |
| $\sigma$ | electrical conductivity |
| $\kappa$ | thermal conductivity |
| $S$ | Seebeck parameter |
| $k_B$ | Boltzmann constant |
| $\chi$ | susceptibility |

**REKA BENTUK III-NITRIDA MENERUSI PENGIRAAN PRINSIP PERTAMA**

## ABSTRAK

Semikonduktor III-nitrida mempamerkan pelbagai ciri yang luar biasa, termasuk liputan spektrum frekuensi yang luas dan rintangan haus yang munasabah. Ini menjadikan mereka bahan yang sesuai dalam pelbagai aplikasi kejuruteraan. Disebabkan keistimewaan ini, kerja penyelidikan yang menyeluruh telah dijalankan ke atas sistem perduaan kumpulan ini sejak beberapa dekad yang lalu. Bagi kes komposit pertigaan, $Al_xGa_{1-x}N$ dan $In_xGa_{1-x}N$ telah dikaji secara menyeluruh manakala pendekatan yang sama tidak berlaku untuk $Al_xIn_{1-x}N$. Banyak kajian telah menunjukkan bahawa penggubalan kualiti $Al_xIn_{1-x}N$ kristal adalah amat mencabar, disebabkan ketidaksepadanan ciri fizikal antara blok induk. Pengetahuan sedia ada mengenai campuran aluminium dan indium boleh memudahkan kerja pengadunan kristal ini. Dengan menggunakan pengiraan evolusi *ab initio*, pencarian menyeluruh untuk komposit stabil AlN-InN telah dilakukan. Pada mulanya, simulasi dijalankan pada tekanan atmosfera, dengan setiap struktur menjalani beberapa peringkat pengoptimuman melalui teori fungsian ketumpatan (density functional theory, DFT). Struktur optimum dipilih berdasarkan nilai kecergasan, iaitu entalpi pembentukan setiap sel unit ($\Delta H_{AlInN}$) manakala struktur kimia yang tidak munasabah (melanggar syarat kekangan) akan dibuang. Pada tekanan atmosfera, pengiraan menyeluruh melahirkan struktur $Al_4In_2N_6$ ($Cmc2_1$) yang stabil secara termodinamik serta lima sebatian metastabil $AlIn_7N_8$ (P3m1), $Al_5InN_6$ (P31m), $Al_2In_4N_6$ (Cc/Aa), $Al_3In_3N_6$ (Cm/Am) dan $Al_6In_2N_8$ ($P2_1$). Pada 2.5 GPa, hanya $Al_7In_2N_9$ (Cm) dan $Al_2In_2N_4$ ($I\bar{4}2d$) dikenalpasti. Struktur pada tekanan 5.0 GPa berkembang ke ortorombik

$Al_4In_2N_6$ ($Cmc2_1$), dua tetragonal $Al_2In_2N_4$ ($I\bar{4}2d$) serta $AlIN_4N_5$ ($I\bar{4}$) dan trigonal $AlIn_5N_6$ ($R3$). Peningkanan tekanan luar melebihi 5.0 GPa didapati menjejaskan kestabilan $Al_xIn_{1-x}N$. Sifat asas fasa stabil dalam komposit $Al_xIn_{1-x}N$ (atmosfera dan tekanan tinggi) kemudiannya disiasat dengan cara DFT dan teori usikan fungsian ketumpatan (density functional perturbation theory, DFPT), semuanya melibatkan penyelesaian hubungan Kohn-Sham. Selepas diperbetulkan dengan kaedah *GW* (Green's function plus screened Coulomb interaction), semua struktur yang tertera di atas mempunyai jurang tenaga dalam julat 0.5-6.0 eV. Kestabilan mekanikal dan dinamik bagi kesemua aloi juga disiasat menerusi pengiraan parameter elastik bebas dan keluk sebaran fonon. Dengan mempertimbangkan kesan "banyak badan", pengiraan optik ke atas fasa atmosfera menunjukkan bahawa indeks biasan had tenaga rendah semakin meningkat dengan penurunan komposisi Al. Had sifar kerentanan tak linear adalah 0.18-120.98 pm $V^{-1}$, menandakan tahap kesan tak linear yang ketara. Tambahan itu, fasa-fasa ini secara intrinsik mempamerkan keluk Seebeck positif yang agak tinggi (199.1-284.6 μV $K^{-1}$) dan $ZT$ ~ 1.0 yang mengalami perubahan kecil dalam julat suhu yang luas 200K - 800K. Penambahan elemen berat seperti In didapati menurunkan kekonduksian haba dan seterusnya menjanakan faktor kuasa yang tinggi (0.019-0.345 W $m^{-1}$ $K^{-2}$). Walaupun penyuntikan lubang berjaya meningkatkan tahap pekali Seebeck bagi setiap fasa, kekonduksian elektrik mereka telah banyak terjejas, menyebabkan faktor kuasa yang lebih rendah. Bagi fasa tekanan tinggi, semua spesies yang dikaji menunjukkan anisotropi elastik yang agak besar dan kekerasan sederhana. Kekerasan Vickers simulasi mereka adalah di antara 9.4 GPa dan 21.6 GPa.

**MATERIAL DESIGN OF III-NITRIDE TERNARY VIA FIRST PRINCIPLES CALCULATIONS**

## ABSTRACT

III-nitride semiconductors exhibit an array of exceptional features, including broad coverage of spectral frequencies range and reasonable wear resistance, making them desirable materials in a variety of engineering applications. Due to these capabilities, extensive researching works have been carried out on their binary systems over the past few decades. In the case of ternary composites, $Al_xGa_{1-x}N$ and $In_xGa_{1-x}N$ are comprehensively studied while the same enthusiasm cannot be said for $Al_xIn_{1-x}N$. Numerous experimental studies have shown that the formulation of a quality $Al_xIn_{1-x}N$ crystal is undeniably challenging, due to mismatch of certain physical properties between its parent blocks. Herein, by applying *ab initio* crossbreed evolutionary computations, extensive search for the thermodynamically and practically stable composites of AlN-InN was performed. Simulations were conducted at atmospheric pressure initially, with each structure underwent several stages of optimization via density functional theory, relaxing its cell shape and internal atoms. Optimized structures were selected based on a fitness value, which is the formation enthalpy per cell ($\Delta H_{AlInN}$) and unrealistic chemical structures violating the constraints would be eliminated. Set at atmospheric pressure, the comprehensive calculations brought forth a thermodynamically stable structure $Al_4In_2N_6$ ($Cmc2_1$) along with five metastable compounds in $AlIn_7N_8$ (P3m1), $Al_5InN_6$ (P31m), $Al_2In_4N_6$ (Cc/Aa), $Al_3In_3N_6$ (Cm/Am) and $Al_6In_2N_8$ ($P2_1$). At 2.5 GPa, only $Al_7In_2N_9$ (Cm) and $Al_2In_2N_4$ ($I\bar{4}2d$) are identified. Candidate structures at 5.0 GPa expanded to orthorhombic $Al_4In_2N_6$ ($Cmc2_1$), two tetragonal $Al_2In_2N_4$

($I\bar{4}2d$) plus $AlIN_4N_5$ ($I\bar{4}$) and trigonal $AlIn_5N_6$ ($R3$). Increasing the pressure beyond 5.0 GPa appears to upset the stability of $Al_xIn_{1-x}N$. Fundamental properties of stable phases within $Al_xIn_{1-x}N$ composites (ambient and high pressures) were then investigated by means of density functional theory (DFT) and density functional perturbation theory (DFPT), mainly solving the Kohn-Sham equation. All structures are revealed to be mixed bonding direct band gap semiconductor with *GW* (Green's function plus screened Coulomb interaction) corrected gap in the range of 0.5 – 6.0 eV. Mechanical and dynamical stabilities of abovementioned alloys are further revealed by the computations of independent elastic parameters and phonon dispersion curves. By considering the many-body effects, optical calculations of atmospheric phases show that both low energy limit of real part and refractive index are increasing monotonically with a decrease in Al composition. Their zero limit nonlinear susceptibilities range from 0.18-120.98 pm $V^{-1}$, denoting a noticeable level of nonlinear effect. Moreover, these phases intrinsically exhibit moderate positive Seebeck curves (199.1 – 284.6 μV $K^{-1}$) and *ZT* close to unity that vary marginally over a broad temperature range of 200K – 800K, demonstrating sign of good bipolar effect tolerance. Addition of heftier element like In yields lower thermal conductivity, which in turn generates high power factor (0.019 – 0.345 W $m^{-1}$ $K^{-2}$) in these alloys. While holes doping enhances the peak Seebeck coefficient of each phase, their electrical conductivity has been greatly compromised, resulting in lower power factor. As for the pressure induced phases, all studied species demonstrate considerable elastic anisotropy and moderate hardness. Their simulated Vickers hardness ranges between 9.4 GPa and 21.6 GPa. In short, theoretical investigation of stable $Al_xIn_{1-x}N$ phases could serve as the catalysis for future experimental synthesis of $Al_xIn_{1-x}N$ system.

# CHAPTER 1 INTRODUCTION

## 1.1 Overview

Generally, $Al_xIn_{1-x}N$ can be regarded as a mixed compound of aluminium nitride and indium nitride with properties characterized by proportion of aluminium to indium. Together with GaN, these two parent blocks (AlN and InN) are exemplifications of III-nitride binary alloys that have drawn enormous researching interests over the past two decades, largely due to their stand-out properties such as unique band gap, high electron mobility [1], good thermal stability [2] and low sensitivity towards ionizing radiations [3]. In the production of optoelectronic devices, a particular energy band gap is often required for the photon absorption or emission mechanism to occur. The direct band gap feature found in most III-V semiconductors makes them an ideal candidate for producing optoelectronic devices with high efficiency of optical absorption or emission. Further discoveries of both novel linear and nonlinear substances are crucial in making sure the continued growth of telecommunications and laser technology fields. Fortunately, efforts expended in researching, synthesizing and identifying new optical materials are very encouraging.

## 1.2 Motivation

Through the use of ternary, tuning of the magnitude of forbidden gap between conduction band and valence band (direct or indirect) is made possible. By and large, direct band gap ternary like $Al_xGa_{1-x}As$, $Al_xGa_{1-x}N$ and $In_xGa_{1-x}N$ are extensively studied. Emerging interest in $Al_xIn_{1-x}P$ [4], an indirect band gap material, has also been noted. However, $Al_xIn_{1-x}N$ does not seem to have the same fate. The lack of exploration for this ternary compound is often attributed to the dissimilarities in covalent bond and thermal stability between AlN and InN, sequentially causing compositional inhomogeneity along with phase separation during alloy formation [5, 6, 7]. Growing

high quality single crystals of these materials is in no doubt an uphill undertaking. Not only that, the understanding of nonlinear characteristics in these materials at microscopic level has also been found wanting. There are many robust first principles techniques that could assist researchers to realize above objectives. These include the configuration interaction (CI) and quantum Monte-Carlo (QMC) approaches. Chiefly among those is the solution of Kohn-Sham equation within density functional theory (DFT) [8, 9]. When incorporated with linear response procedures, elucidation of various optical spectrums is made possible. One particular weakness is the underestimation of energy band gap, thus causing the absorption to start at very low energy. Reason being that the Kohn-Sham formulism only deals with ground state properties and as such neglects the unoccupied conduction bands.

In spite of the difficulties, interest on $Al_xIn_{1-x}N$ related studies continue to be revived sporadically [10, 11, 12]. This material remains an enticing prospect, owing to its wide coverage of electromagnetic spectrum ranging from deep ultraviolet to near infrared region. Though experimental approach targeting photoluminescence excitation of $Al_xIn_{1-x}N$ has been done [13], other key optical properties like refractive index and absorption pattern are still unexplored. Due to their likely wide energy band gap range, $Al_xIn_{1-x}N$ compounds are believed to be prospective thermoelectric materials [14]. Having a thermoelectric device that efficiently recycles waste energy would be mouth-watering as it not only opens pathway for sustainable system development but also promotes green energy concept. While extensive investigations have been performed for thermoelectric behaviours of tetrahedrite, half Heusler [15, 16, 17] and IV tellurite based compounds [18], the desire for materials with multiple interesting properties has seen a change of focus for III-nitride alloys. III-nitride thermoelectric materials are flexible in the sense that they can be directly combined

with akin device technology, providing active thermal removal and efficiency improvement in nitride-based high power density instruments [19]. Improved figure of merit has also been demonstrated in III-nitride materials that underwent alloy tuning. Distinction of thermal conductivity with the mass fraction $x$ has been highlighted in III-nitride ternary such as $Al_xGa_{1-x}N$ [20, 21] and $In_xGa_{1-x}N$ [22]. Despite the projected optical and optoelectronic potential of AlN-InN system, studies with regard to $Al_xIn_{1-x}N$ thermoelectric efficiency are relatively rare.

In sight of the aforementioned constraints, the need to search for possible stable and metastable crystal structures within Al-In-N system by means of theoretical forecast has become vastly momentous. By identifying an array of probable structures hypothetically, each with reliable and promising composition breakdown, the characterization and synthesis of $Al_xIn_{1-x}N$ might become more achievable. With reference to the predicted Al/In ratio, one can eliminate the possibility of having a compound grown from unreasonable initial condition. Thus far, there have been quite a number of theoretical investigations on lattice parameters and band gap energies of $Al_xIn_{1-x}N$. Most of these calculations were performed by assuming that the relaxed lattice parameters of $Al_xIn_{1-x}N$ alloys, in either wurtzite or zincblende form, are expressible as a linear combination of the lattice constants of their respective binaries [23, 24, 25]. While optimization of these alloys was later carried out and their respective elastic parameters have been compared to the necessary stability criteria, information about their individual formation enthalpy is not available. Conjecturing the structures of ternary $Al_xIn_{1-x}N$ alloys without performing structural search and multiple relaxations is incorrect. Structures to be studied must be at least metastable, if not thermodynamically stable. This can be verified by performing a thorough search for whole composition range ($x$ = 0-1) and comparing the formation enthalpy of each

fit structure. Moreover, foretold global minimum and practically stable crystals must refrain from undergoing further structural transition should the surrounding temperature changes. This uncertainty can be checked by analyzing the phonon frequencies and eigenvectors of a chosen structure, within its Brillouin zone. Mechanical stability that indicates reaction against external disturbance should also be tested. A structure is said to be mechanically unstable if its capability to return to equilibrium position is loss when being disturbed by an extraneous action.

### 1.3 Objectives

To summarize, research objectives of this work are twofold. In the primary section, screening of novel stoichiometric phases within $Al_xIn_{1-x}N$ composites at atmospheric and high pressures are to be carried out using state-of-the-art calculations. This has been done by means of prediction-specific evolutionary algorithm plus first principles scheme in the form of the density functional approach. Next, fundamental properties of stable phases within $Al_xIn_{1-x}N$ composites (ambient and high pressures) will be investigated via the use of DFT and density functional perturbation theory (DFPT). Apart from acquiring ground state property such as density of states and electronic band structure, response of stable stoichiometries towards higher energy orders has also been performed, activating the computation of their respective band gap correction and crucial characteristics like optical, elastic, piezoelectric properties. And with the ongoing large scale application of semiconductor devices in wireless data transfer, industrial control coordination and scientific study, urgent demands for highly versatile and effective self-powered electronic appliances should thrust researchers into exploring multifunctional materials that possess multiple outstanding properties. Through this work, it is hoped that the theoretical investigations of steady $Al_xIn_{1-x}N$ composites and their various natural characteristics could lay the foundation for

creation of multifunctional devices in which the electronic, optical, thermoelectric, piezoelectric and other properties can be coupled to one another.

### 1.4 Thesis outline

The thesis outline can be divided into three parts. In the first section, detailed formalisms and calculational techniques are presented. The second part concerns the screening of various stable $Al_xIn_{1-x}N$ stoichiometries at atmospheric pressure and calculation of their important properties. Finally, the last part addresses the extension of $Al_xIn_{1-x}N$ prediction under high pressure condition.

# CHAPTER 2 THEORIES AND MODELS

## 2.1 Overview

The screening of ground state and metastable structures within $Al_xIn_{1-x}N$ system was conducted via Universal Structure Predictor: Evolutionary Xtallography or popularly known as USPEX code [26, 27, 28]. First-principles approach and density functional theory are the fundamental ingredients used in contriving its evolutionary algorithm. Details on the execution plan of USPEX starting from general chemical input to finalizing structure selection will be explored in this chapter. Fundamental properties of forecasted stable phases within $Al_xIn_{1-x}N$ composites (ambient and high pressures) will then be investigated by means of DFT and density functional perturbation theory (DFPT) [29], mainly solving the Kohn-Sham equation.

## 2.2 Searching operation

By providing raw information such as types of elements and their exact constituents, USPEX automatically append the default atom dependent hard constraints such as initial unit cell volume and minimum separation between atoms. Constraints are helpful in maintaining the stability of total energy calculations and relaxation, through elimination of redundant and unreasonable nonphysical structures. A group of random structures that gratify above constraints are created. These structures will be stored in the first generation and each undergoes gradual optimization. Filtration of structures based on chosen optimization property (fitness) is done. Fitness can be in the form of enthalpy (default selection), volume, hardness, band gap or magnetic moment. Unfit structures are discarded while those deemed fit will play the role of parent. A structure has high fitness if its chances to last until the

next generation are high. Fresh structure is formed from parent through any of the following variant operators.

### 2.2.1 Heredity

Comprehensible planar slices of two parent structures are combined. The participating parent structure stores important information like relative position of proximate atoms. Lattice constants of the offspring are obtained by performing weighted arithmetic mean on lattice vectors of parent, where structure with greater vector matrices contributes more heavily.

### 2.2.2 Softmutation

Parent structure is altered as a result of large atomic displacements along the eigenvectors of softest phonon modes.

### 2.2.3 Lattice mutation

Lattice vectors of the parent structure are changed by applying a symmetric strain matrix. This operator helps to minimize events of untimely convergence towards a particular lattice of an immature structure.

### 2.2.4 Transmutation

Offspring is achieved by turning randomly chosen atoms within a parent structure into other chemical species present in it.

Candidates for new structures that satisfy the hard constraints are moved into new generation. Random structures can be concurrently added in an attempt to reduce the impact of trapped local optimization. Optimizing the atomic coordinates and lattice parameters of each candidate creates new individual. Local optimization processes continue until the user specified number of new individuals is reached. At this stage, new individuals will assume the parental role and take part in aforementioned steps.

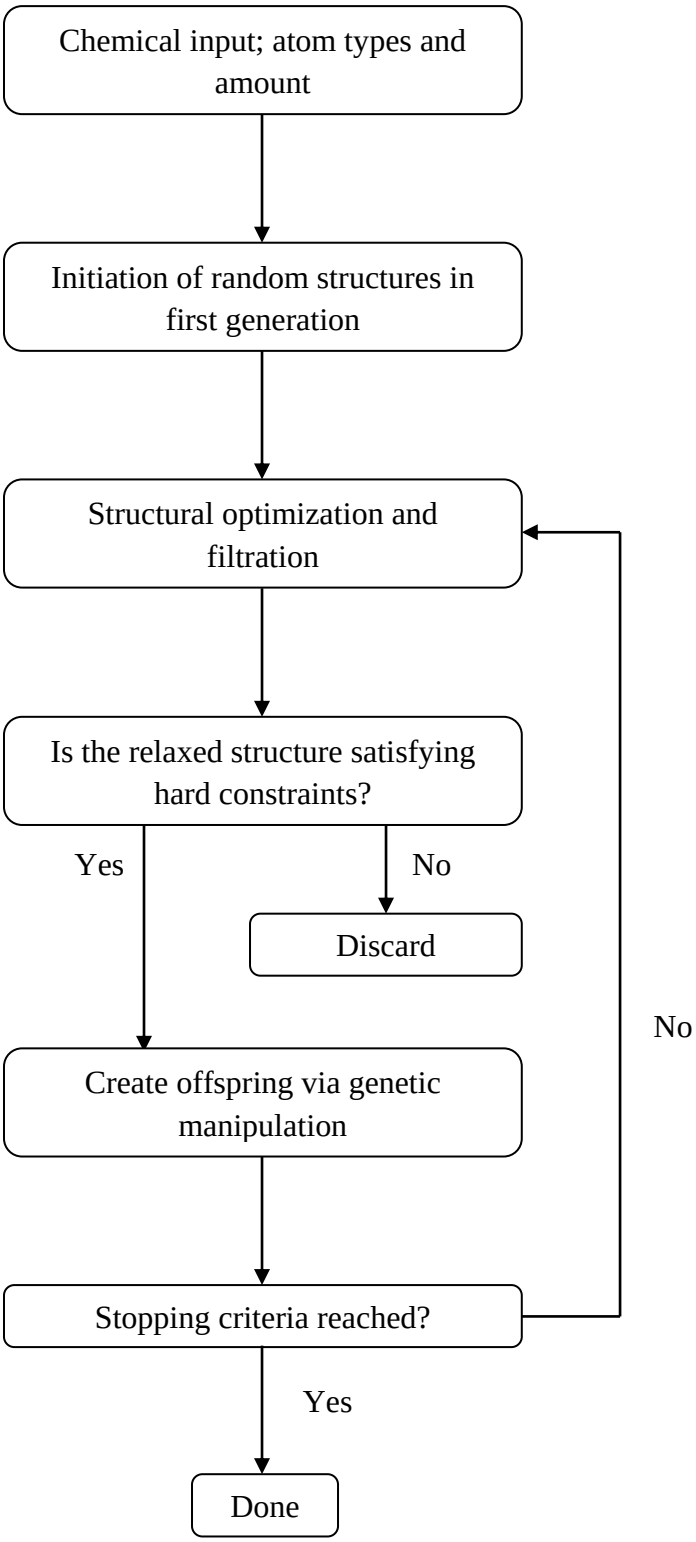


**Figure 2.1** Evolutionary algorithm implemented in USPEX

This course of action is repeated until all the selected low enthalpy individuals can no longer be mutated. Overall flow of evolutionary algorithm implemented in USPEX is summarized below. Above procedures will be repeated for simulations at higher pressures (2.5, 5.0, 10.0 and 20 GPa).

**2.3 Ab initio approach**

Important properties of materials are influenced by the behavior of its internal atoms. Numerous models have been used to describe the interaction among atoms within a solid [30]. While classical assumptions such as the Monte Carlo model and *ab initio* molecular dynamics model are capable of researching matter at microscopic level, their computational cost is often expensive. As such, the equally efficient and computationally cheaper first-principles approach based on quantum mechanics has become a popular choice. This method enables researchers to predict important properties of substances even before the synthesis works take place. The electron theory of quantum mechanics has for decades, served as fundamental theory in wide areas of science and engineering that include condensed matter physics, nuclear physics, photonics and many more. The integral part of quantum mechanics is Schrodinger equation [31], which describes the relationship between wave function and movement of microscopic particles under the presence of external potential $V(\boldsymbol{r})$. The general Schrodinger equation for a system comprised of multiple atoms forming a solid crystal, can be written as

$$H\Psi=E\Psi \qquad \text{(Eq. 2.1)}$$

where $H$ is the Hamiltonian operator, $E$ is the eigenvalue and $\Psi$ is the orbital wave function. This operator is made up of five terms, namely the total kinetic energy of every single electron, potential energy of the interaction between electrons with atomic nuclei, energy of interaction between dissimilar electrons, total kinetic energy

of every nucleus and lastly interaction between all nuclei. It is presupposed that Schrodinger equation can be rightly solved with normalization condition on wave functions

$$\langle \varphi_i | \varphi_i \rangle = 1 \qquad \text{(Eq. 2.2)}$$

satisfied. By solving the Schrodinger equation, one can unlock crucial details like atomic structures and density of states of a system, hence making the physical and chemical processes in the system accessible. However, providing solution to Schrodinger equation for multi-particle systems is no doubt difficult and complex. Segregation of Schrodinger equation into independent terms is not possible due to the presence of electron-electron interrelation in its Hamiltonian term, that is non-local in nature. Mathematically justified approximation methods have since been introduced so as to simplify the solution of many body systems' Schrodinger equation.

In Born-Oppenheimer approximation [32], heavier nuclei are assumed to be moving at very slow pace. Their kinetic energy contribution becomes negligible and thus can be omitted from the Hamiltonian. Under this approximation, separate treatment of nuclei and electrons can be realized. With the Hamiltonian simplified, a more straightforward solution of Schrodinger equation is expected. But this is not the case. Aforesaid complication remains because electron-electron term is yet to be removed. Hartree-Fock approximation [32] on the other hand replaces the multi particle systems wave function with product of single electron wave function. Hamiltonian is further abbreviated with only kinetic energy of the electrons, potential energy due to nuclei-electrons interaction and potential energy of electron-electron repulsion terms left. Electrons in this model are seen as drifting in both ion and mean potential fields of surrounding electrons. This approximation however disregards the

permutation among neighboring electrons and at times reproduces hard to access excited states, therefore affecting the precision of computing outcome. More auxiliary approximations were needed to reduce the complexity in solving Schrodinger equation. A breakthrough was attained with the introduction of density functional theory (DFT). At this instance, electronic density has replaced many electron wave function as the fundamental variable.

$$E[n(\boldsymbol{r})] = \langle\varphi|H|\varphi\rangle = F[n(\boldsymbol{r})] + \int V_{ext} n(\boldsymbol{r}) d^3r \qquad \text{(Eq. 2.3)}$$

*F[n(**r**)]* is a universal functional that represents contributions from kinetic and other potential energies. Revamp of many body problem with regard to density is depending on Hohenberg-Kohn theorems [33] and Kohn-Sham formulation. The former can be explained using the following two attestations.

**Theorem 1**

When a system of interacting constituent parts is under the effect of an external potential $V_{ext}(\boldsymbol{r})$, its density of ground state $n_0(\boldsymbol{r})$ is completely and distinctively correlated to $V_{ext}(\boldsymbol{r})$. To gain better insight, let us assume there are two diverse peripheral potentials $V_{ext}^{(1)}(\boldsymbol{r})$ and $V_{ext}^{(2)}(\boldsymbol{r})$, where both yield the same ground state density. Due to different Hamiltonians $\left(H^{(1)} \text{ and } H^{(2)}\right)$, these potentials bound to have different ground wave function $\left(\varphi_i^{(1)} \text{ and } \varphi_i^{(2)}\right)$. Therefore,

$$\begin{aligned} E^{(1)} &= \langle\varphi^{(1)}\left|H^{(1)}\right|\varphi^{(1)}\rangle \\ &< \langle\varphi^{(2)}\left|H^{(1)}\right|\varphi^{(2)}\rangle \\ &< \langle\varphi^{(2)}|H^{(2)}|\varphi^{(2)}\rangle + \langle\varphi^{(2)}|H^{(1)} - H^{(2)}|\varphi^{(2)}\rangle \\ E^{(1)} &< E^{(2)} + \int \left[V_{ext}^{(1)} - V_{ext}^{(2)}\right] n_0(\boldsymbol{r}) d^3r \end{aligned}$$

Likewise,

$$E^{(2)} < E^{(1)} + \int \left[V_{ext}^{(2)} - V_{ext}^{(1)}\right] n_0(\boldsymbol{r}) d^3r$$

Adding the two inequalities above gives an unempirical relationship in which $E^{(1)} + E^{(2)} < E^{(2)} + E^{(1)}$. It is therefore not reasonable for unlike external potentials to have the same $n_0(\boldsymbol{r})$.

**Theorem 2**

Numerical statements from first theorem show that the correlation between charge density and external potential is of one to one function. As such, $E[n(\boldsymbol{r})]$ is logically a minimum if and only if $n(\boldsymbol{r}) = n_0(\boldsymbol{r})$.

In Kohn-Sham DFT calculations, permutation among electrons is represented by electron density functional $n(\boldsymbol{r})$. It is deduced that the ground state energy and charge density of interacting electrons are similar to those of non-interacting electrons. Complications arise from interaction of electrons are simplified as movement of non-interacting electrons within an effective potential field. Ground state energy of this system is derivable through minimization of the following functional:

$$E[n(\boldsymbol{r})] = \int V_{eff}(\boldsymbol{r}) n(\boldsymbol{r}) d^3r + T[n(\boldsymbol{r})] \qquad \text{(Eq. 2.4)}$$

where $T[n(\boldsymbol{r})]$ is the non-interacting kinetic energy. Particles no longer depend on each other. Electronic system as a whole can now be expressed by a solitary product of individual wave function. Density distribution $n(\boldsymbol{r})$ can be determined using

$$n(\boldsymbol{r}) = \sum_{i}^{N} |\varphi_i(\boldsymbol{r})|^2 \qquad \text{(Eq. 2.5)}$$

and with that wave functions of every electron state are incorporated. This means electronic charge density is evaluated by considering non interacting system as sum

over all occupied single orbital densities. Principally, atoms always align themselves in regular and replicating patterns. These periodicities also lead to regularities in potential, charge density and later stage the wave functions. Since $\varphi_i(\boldsymbol{r})$ is periodic, Fourier series can be applied to expand it. In order to construct the density, $\varphi_i(\boldsymbol{r})$ need to be integrated over all possible wave vectors. Plane wave is expanded to the limit of cut-off energy. Wave functions surrounding the nuclei vary rapidly due to strong potential. These wave functions usually do not contribute much, only affecting the mechanical, chemical and electronic properties marginally. As such, it is possible to replace the potential near nuclei with weaker but smoother potential known as pseudopotential. The pseudopotential wave functions do not vary as swiftly as those nearby the nuclei. Lower cut-off energy can now be used to reduce the expansion space. In short, DFT converts a many body systems into single body systems by ousting the interaction potential between electrons. Equation of Kohn-Sham can be written as:

$$\left[-\frac{\hbar}{2m}\nabla^2 + V_{eff}(\boldsymbol{r})\right]\varphi_i = E_i\varphi_i \qquad \text{(Eq. 2.6)}$$

The single particle effective potential is expressible as:

$$V_{eff}(\boldsymbol{r}) = V_{ion}(\boldsymbol{r}) + V_H(\boldsymbol{r}) + V_{xc}(\boldsymbol{r}) \qquad \text{(Eq. 2.7)}$$

The three terms in sequential refer to electron-nuclei Coulomb potential, classical electronic Coulomb potential and exchange-correlation potential which covers all quantum mechanical effects. Unlike previous models, solution to Kohn-Sham equation centralizes around the exchange correlation energy. True form of this energy is nonetheless unknown. For that reason, engaging an appropriate form of exchange correlation energy functional is extremely critical in ensuring high precision and accuracy of DFT calculations. Two common choices of exchange-correlation approximation are the local density approximation (LDA) and

generalized gradient approximation (GGA). LDA assumes that the density of exchange-correlation energy at every position for a particle is akin to the uniform electron gas with similar density found at that point. This approximation will be flawless if there are no inhomogeneities in electron density around a position, but actual electronic densities are far from being uniform. GGA is able to include the effects of inhomogeneities by adding a correction term know as local gradient to existing LDA functional. Moreover, its lower exchange energy indirectly reduces the binding energy, hence complementing the over binding result in LDA. A popular GGA functional constructed on the root of this model is PBE functional, which is one of the GGA functionals that has been utilized broadly at present. Once the decisive factor on approximation has been fixed, solution of Kohn-Sham equation can be carried out. Generally, the Kohn-Sham equation is solved using a self-consistent manner. After picking the proper approximation, single electron wave function $\varphi_i(\boldsymbol{r})$ obtained through substitution of a user defined trial electron density $n(\boldsymbol{r})$ into equation 2.4 is used to reevaluate an improved $n(\boldsymbol{r})$ by means of equation 2.4. If the new $n(\boldsymbol{r})$ differs from initial $n(\boldsymbol{r})$, it will be taken as input to solve the two equations above again. This iteration course is repeated until the difference between trial and computed electron densities is within the preset convergence criteria. The converged electron density is then used to calculate total energy of the desired system. Highlight of steps needed for solving Kohn-Sham equation can be seen in **Figure 2.2**. The main idea here is to treat the electron density as a basic variable to disentangle the universal many body Schrodinger equation. Accomplishing self-consistency can be a really demanding because it is obligatory to pick a suitable alternative for updating either the potential or charge density in each iteration of the

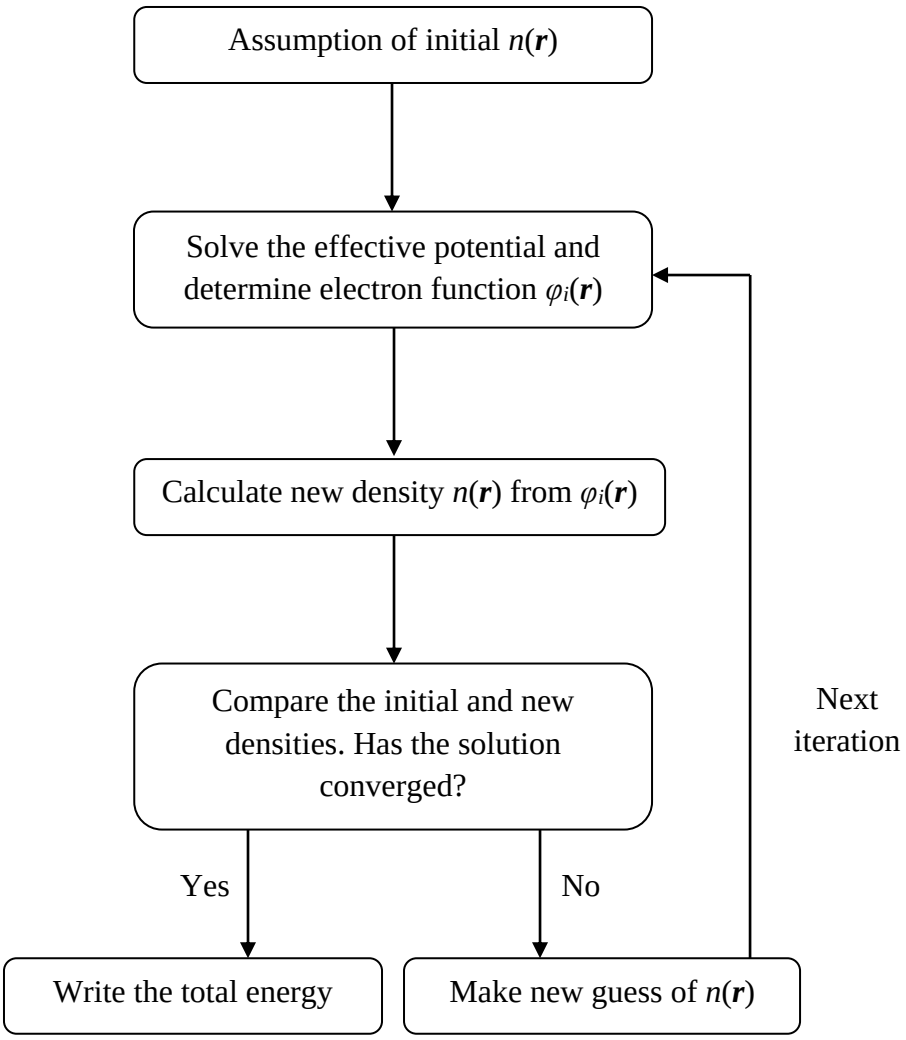


**Figure 2.2** Self-consistent procedure used in solving Kohn-Sham equation

previous step. It is less complex to portray in term of the electronic density, which is exclusive, whereas the external potential is unique modulo a constant. During the solution of Kohn-Sham ansatz, only ground state properties are determined as the exchange correlation potential used is an explicit function of ground state densities. Failures in the representation of electronic excited states have been documented. These setbacks can be overcome using quantum formulism for perturbation theory, within the DFT framework. Density functional perturbation theory (DFPT) exploits the good delineation of ground state in DFT to accurately portray the down tempo excitation in low energy region. By gently perturbing the electronic ground state, wide range of physical properties become quantifiable through the total energy derivatives generated. Perturbation [34] can be in the form of atomic displacements, homogenous electric or magnetic fields, strain and alchemical change. Every perturbation begins with the classification of an enormously undersized parameter. Taking λ as the diminutive parameter, the perturbed Schrodinger equation can be written as

$$H_\lambda = H + X_\lambda \qquad \text{(Eq. 2.8)}$$

where $H$ and $X_\lambda$ are the unperturbed Hamiltonian and external perturbed quantity, respectively. The ambiguous perturbed quantities $X_\lambda$ can be expanded to produce a linearly increasing term in the form of

$$X_\lambda = \lambda X^{(1)} + \lambda^2 X^{(2)} + \lambda^3 X^{(3)} + \cdots \qquad \text{(Eq. 2.9)}$$

Apart from Hamiltonian term, $X$ can also be used to signify the electronic energy $E$, electronic wavefunctions $\varphi(\boldsymbol{r})$, external potential $V(\boldsymbol{r})$ and electron charge density $n(\boldsymbol{r})$. When expanded into the powers of λ, their respective complete form can be rewritten as

$$E_\lambda = E + \lambda \frac{\delta E(\boldsymbol{r})}{\delta \lambda} + \lambda^2 \frac{\delta^2 E(\boldsymbol{r})}{\delta \lambda^2} + \lambda^3 \frac{\delta^3 E(\boldsymbol{r})}{\delta \lambda^3} + \cdots \qquad \text{(Eq. 2.10)}$$

$$\varphi_\lambda(\boldsymbol{r}) = \varphi(\boldsymbol{r}) + \lambda\frac{\delta\varphi(\boldsymbol{r})}{\delta\lambda} + \lambda^2\frac{\delta^2\varphi(\boldsymbol{r})}{\delta\lambda^2} + \lambda^3\frac{\delta^3\varphi(\boldsymbol{r})}{\delta\lambda^3} + \cdots \quad \text{(Eq. 2.11)}$$

$$V_\lambda(\boldsymbol{r}) = V(\boldsymbol{r}) + \lambda\frac{\delta V(\boldsymbol{r})}{\delta\lambda} + \lambda^2\frac{\delta^2 V(\boldsymbol{r})}{\delta\lambda^2} + \lambda^3\frac{\delta^3 V(\boldsymbol{r})}{\delta\lambda^3} + \cdots \quad \text{(Eq. 2.12)}$$

$$n_\lambda(\boldsymbol{r}) = n(\boldsymbol{r}) + \lambda\frac{\delta n(\boldsymbol{r})}{\delta\lambda} + \lambda^2\frac{\delta^2 n(\boldsymbol{r})}{\delta\lambda^2} + \lambda^3\frac{\delta^3 n(\boldsymbol{r})}{\delta\lambda^3} + \cdots \quad \text{(Eq. 2.13)}$$

Linearization of previously discussed ground state density and Kohn-Sham orbitals leads to charge density linear response and Kohn-Sham derivatives:

$$\frac{\delta n(\boldsymbol{r})}{\delta\lambda} = 4Re\sum_i \varphi_i^*(\boldsymbol{r})\frac{\delta\varphi_i(\boldsymbol{r})}{\delta\lambda} \quad \text{(Eq. 2.14)}$$

$$(H - E_i)\frac{\delta\varphi_i(\boldsymbol{r})}{\delta\lambda} = -\left(\frac{\delta V_{eff}(\boldsymbol{r})}{\delta\lambda} - \frac{\delta E_i}{\delta\lambda}\right)\varphi_i(\boldsymbol{r}) \quad \text{(Eq. 2.15)}$$

where

$$\frac{\delta V_{eff}(\boldsymbol{r})}{\delta\lambda} = \frac{\delta V_{ion}(\boldsymbol{r})}{\delta\lambda} + \int\frac{e^2}{|\boldsymbol{r}-\boldsymbol{r}'|}\frac{\delta n(\boldsymbol{r}')}{\delta\lambda}d\boldsymbol{r}' + \frac{\delta V_{xc}(\boldsymbol{r})}{\delta n(\boldsymbol{r}')}\frac{\delta n(\boldsymbol{r}')}{\delta\lambda}d\boldsymbol{r}' \quad \text{(Eq. 2.16)}$$

Note that $\Delta V_{eff}(\boldsymbol{r})$ is a linear functional of $\Delta n(\boldsymbol{r})$ which consecutively depends on variation of Kohn-Sham orbitals. As such, calculation of self consistency can be performed for generalized linear problems. In addition, the linear response technique [30] enables the calculation of the dynamical matrix at arbitrary *q* vectors.

### 2.3.1 Lattice dynamics

In phonon calculation, atomic displacements are treated as perturbations. Self consistent computation is applied to the electronic response of perturbation. When nuclei are not at their equilibrium coordinate, forces which are opposite of the energy derivative appear. These interatomic forces are linearly correlated to the displacement of each nucleus. For crystal consideration, phonons are ruled by wave vector $\boldsymbol{q}$. The displacement patterns of *x*-th atom in $\alpha$-th Cartesian component, $U_x^\alpha(\boldsymbol{q})$ and phonon frequencies, $\omega(\boldsymbol{q})$ are expressible using the secular equation:

$$\sum_{y,\beta}\left(C_{xy}^{\alpha\beta}(\boldsymbol{q}) - M_x\omega^2(\boldsymbol{q})\delta_{xy}\delta_{\alpha\beta}\right)U_y^{\beta}(\boldsymbol{q}) = 0 \qquad \text{(Eq. 2.17)}$$

where $C_{xy}^{\alpha\beta}(\boldsymbol{q})$ is the matrix of inter atomic force constants. DFPT enables an efficient calculation of second order energy derivatives, required to generate the dynamical matrices.

$$C_{xy}^{\alpha\beta}(\boldsymbol{q}) = \frac{1}{n}\left(\frac{\delta^2 E}{\delta u_x^{\alpha}(\boldsymbol{q})\delta u_y^{\beta}(\boldsymbol{q})}\right) \qquad \text{(Eq. 2.18)}$$

First order derivative of electronic energy is computable without the knowledge of any first order quantity. Dynamical matrix due to second order change in total energy is depending on the variation of first order electronic charge density.

$$\frac{\delta^2 E}{\delta\lambda^2} = \int \frac{\delta V(\boldsymbol{r})}{\delta\lambda}\frac{\delta n(\boldsymbol{r})}{\delta\lambda}\,d\boldsymbol{r} + \int n(\boldsymbol{r})\frac{\delta^2 V(\boldsymbol{r})}{\delta\lambda^2}\,d\boldsymbol{r} \qquad \text{(Eq. 2.19)}$$

This result is expandable to derivatives of mixed perturbation.

$$\frac{\delta^2 E}{\delta\lambda\delta\mu} = \int \frac{\delta V(\boldsymbol{r})}{\delta\lambda}\frac{\delta n(\boldsymbol{r})}{\delta\mu}\,d\boldsymbol{r} + \int n(\boldsymbol{r})\frac{\delta^2 V(\boldsymbol{r})}{\delta\lambda\delta\mu}\,d\boldsymbol{r} \qquad \text{(Eq. 2.20)}$$

The interatomic force constants are obtained by the use of fast Fourier transform (FFT) of the dynamical matrices in real space super cell, covering a grid in Brillouin zone. Within the real space, hidden dynamical matrices in reciprocal space (not necessarily contained in the original grid) can be uncovered at any wave vector. Removing the long range component of real space force constants allows the use of a coarser reciprocal space grid during Fourier interpolation. Inverse Fourier transform is then performed on these force constants so as to obtain the phonon frequencies at arbitrary points in reciprocal space, via interpolation. One can verify the dynamical stability of a system by probing the presence of negative phonon frequencies or soft mode within the phonon dispersion curve. Appearances of soft modes within a

structure indicate crystal instability. Structure concerned prevents this scenario by bestowing a new form, which is more conducive to lattice stability.

### 2.3.2 Mechanical properties

Elastic parameters can be denoted as force constants connected to homogenous strains. Integrating DFPT for homogenous distortions [30] requires the inclusion of a transitional conjured Hamiltonian which is associated to unperturbed system. When a crystal is dilated with amplitude of *x*, its strained Hamiltonian becomes

$$H^x = -\frac{\hbar}{2m}\nabla^2 + V_{ion}^x(\boldsymbol{r}) + e^2\int\frac{n^x(\boldsymbol{r}')}{|\boldsymbol{r}-\boldsymbol{r}'|}dr' + V_{xc}\left(n^x(\boldsymbol{r}')\right) \quad \text{(Eq. 2.21)}$$

in which

$$V_{ion}^x(\boldsymbol{r}) = \sum_{ls} V_s(\boldsymbol{r} - x\boldsymbol{R}_l - x\boldsymbol{T}_m) \quad \text{(Eq. 2.22)}$$

$\boldsymbol{R}_l$ is the site of *l*-th unit cell within Bravais lattice while $\boldsymbol{T}_m$ is the *m*-th atom inside the unit cell. The intermediate conjured Hamiltonian, $\widetilde{H}^x$, is then derived from unperturbed Hamiltonian, through a scale conversion:

$$\widetilde{H}^x\left(\boldsymbol{r}, \frac{\delta}{\delta\boldsymbol{r}}\right) = H\left(\frac{\boldsymbol{r}}{x}, x\frac{\delta}{\delta\boldsymbol{r}}\right) \quad \text{(Eq. 2.23)}$$

Both conjured and real strained Hamiltonians have identical boundary conditions, thus permitting the use of DFPT in relative energy difference calculation. Other quantities of $\widetilde{H}^x$ and *H* that are inconsequentially allied are:

$$\tilde{E}_i^x = E_i \quad \text{(Eq. 2.24)}$$

$$\tilde{\varphi}_i^x(\boldsymbol{r}) = x^{-\frac{3}{2}}\varphi_i\left(\frac{\boldsymbol{r}}{x}\right) \quad \text{(Eq. 2.25)}$$

$$\tilde{n}^x(\boldsymbol{r}) = x^{-3}n\left(\frac{\boldsymbol{r}}{x}\right) \quad \text{(Eq. 2.26)}$$

Computation of energy variation due to strain involves a two steps procedure. Firstly, energy distinction between unperturbed and fictitious strained crystals is calculated.

This is then followed by calculation of energy difference between the latter and the actual strained crystals by means of perturbation approach. Energy variation between conjured and real strained crystals can now be evaluated. In principal, perturbed atoms will realign themselves in order to minimize the energy sum as a function of applied strain. For every applied strain, atoms are relaxed to their energetically preferred lattice positions. During relaxations, perturbed lattice vectors are fixed. The distortion in energy is used to characterized elastic moduli $C_{ij}$ through the relationship

$$\Delta E \propto \sum_{i=1}^{6}\sum_{j=1}^{6} C_{ij}\varepsilon_i\varepsilon_j \qquad \text{(Eq. 2.27)}$$

where $\varepsilon_i$ refers to the $i$ th constituent of strain tensor in Voigt notation, with specific designations of $xx$ = 1, $yy$ = 2, $zz$ = 3, $yz$ = 4, $xz$ = 5 and $xy$ = 6. By adding another perturbation quantity in electric field, piezoelectric property can be further evaluated. Piezoelectricity can be viewed as a bridge linking the interchange effect between mechanical and electrical properties. We regard a material as having piezoelectric potential if its piezoelectric effect is favourable. Other constraints to be fulfilled [35] are:

- Absence or lack of inversion symmetry. Structures with space group of 1, 3-9, 16-46, 75-82, 89-122, 143-146, 149-161, 168-174, 177-190, 195-199, 207-220 are said to be non-centrosymmetric.
- Energy band gap > 0.1 eV
- Number of atom per unit cell ≤ 20

Describing the piezoelectric effect requires adequate knowledge of piezoelectric stress coefficient, $e_{ij}$. These $e_{ij}$ parameters are reckoned through straightforward computations of change in polarization intensity in the $i$-th direction when being

strained in the *j*-th route. Piezoelectric coefficients are defined as contributions from relaxed (internal strain) and clamped ion terms. These parameters can be represented by a $3 \times 3$ matrix, consisting of eighteen third ranked tensors. Some of these tensors could be equal to zero or identical to each other, due to constraint imposed by individual crystal's point group symmetry.

$$e_{ij} = e_{ij}\,(clamped\ ion) + e_{ij}\,(relaxed\ ion)$$

$$e_{ij} = \begin{bmatrix} e_{11} & e_{12} & e_{13} \\ e_{21} & e_{22} & e_{23} \\ e_{31} & e_{32} & e_{33} \end{bmatrix} \qquad \text{(Eq. 2.28)}$$

The subscript *i* signifies direction along the three axes while *j* is the pairs of Cartesian direction expressed in Voigt notation. Self consistent calculations are performed on electronic response to these perturbations, creating first and second order energy derivatives of occupied wave functions. Energy derivatives that correspond to strain and electric field produce the clamped ion component. During this stage, movements of atoms or ions are not permitted. Only response with respect to electric field relaxation is taken into account. In contrast, derivatives that depend on strain and atomic displacement generate the relaxed ion part. Summation of the former and latter terms gives rise to total piezoelectric coefficient. While most non-centrosymmetric composites have dominant positive coefficients in which charges are induced during extension, some appears to be solely responsive towards compression, due to their large negative coefficients.

### 2.3.3 *GW* correction

Despite its directness and wide application, DFT has a tendency to undervalue the energy band gap of most materials. On the whole, Kohn-Sham formulism is very much depending on the correlation between definite N electron system and its unreal non-interacting counterpart through *xc* potential, an explicit

ground state functional. As a result, attempt to mirror the N body quantum mechanical problem onto N number of 1-body problems becomes less efficient. Furthermore, the connection between electron density and exchange correlation in Kohn-Sham ansatz is highly non-analytical and non-local. A slight variation in $n(\boldsymbol{r})$ affects *xc* greatly, making the construction of a complete reliable approximation to exact *xc* at further points extremely difficult. The contribution of *xc* discontinuity to energy band gap is often neglected in such manner. A way to tackle this woe is by implementing perturbation theory within *GW* approximation [36]. In *GW* method, electronic self energy is approximated as the product of Green's function *G* and screened interaction *W* among quasiparticles. When photon incidents on a compound and expels an electron, the system gains additional electron. Coulomb interaction between the newly injected electron and neighbouring polarization cloud forms quasiparticle, which can be depicted as a unit comprising of electrons and holes cloud, as shown in **Figure 2.3**.

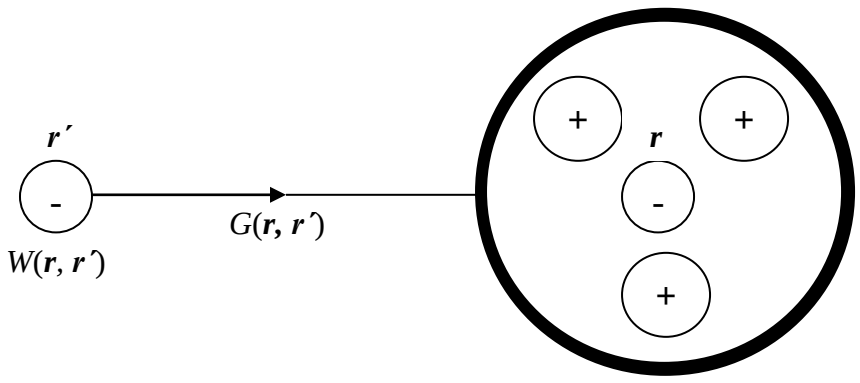


**Figure 2.3** Screened interaction

Holes surrounding the electron at $\boldsymbol{r}$ shield its bare Coulomb potential $\upsilon(\boldsymbol{r}, \boldsymbol{r}')$, hence producing the effective potential at $\boldsymbol{r}'$, given by screen interaction $W$. Quasiparticles act reciprocally by way of screened interaction $W$ instead of the robust Coulomb interaction. With that, the energies $E_i$ and wave functions $\varphi_i$ are at this time governed by the quasiparticle relation

$$H(\boldsymbol{r})\varphi_i(\boldsymbol{r}) + \int \sum (\boldsymbol{r}, \boldsymbol{r}', E_i/h)\varphi_i(\boldsymbol{r}')d^3r' = E_i\varphi_i(\boldsymbol{r}) \qquad \text{(Eq. 2.29)}$$

Approximating $\varphi_i(\boldsymbol{r})$ and $\sum(\boldsymbol{r}, \boldsymbol{r}', E_i/h)$ to $\mu_i^{KS}(\boldsymbol{r})$ and $V_{xc}(\boldsymbol{r})$ will enable the exploitation of Kohn-Sham equation

$$H\varphi_i^{KS}(\boldsymbol{r}) + V_{xc}(\boldsymbol{r})\varphi_i^{KS}(\boldsymbol{r}) = E_i^{KS}\varphi_i^{KS}(\boldsymbol{r}) \qquad \text{(Eq. 2.30)}$$

Upon configuring the ground state, Green's function is set up. This is followed by computation of screened interaction $W$. In terms of dielectric function,

$$W = \int\int \epsilon(\boldsymbol{r}, \boldsymbol{r}', E)\, \nu(\boldsymbol{r}, \boldsymbol{r}')d\boldsymbol{r} \qquad \text{(Eq. 2.31)}$$

The Random Phase Approximation (RPA) [37] is used to determine the dielectric function $\epsilon(\boldsymbol{r}, \boldsymbol{r}', E)$ and finally leads to quasiparticle energy solution

$$E_i = E_i^{KS} + Z_i\langle\varphi_i^{KS}|\sum^{GW} - V_{xc}|\varphi_i^{KS}\rangle \qquad \text{(Eq. 2.32)}$$

where $\sum^{GW}$ = $GW$ self energy and $Z_i$ is the renormalization factor. Segregation of the one shot $GW$ into both exchange and correlation parts can now be done, denoted by $\sum_x^{GW}$and $\sum_c^{GW}$. The band gap correction or scissor shift, when integrated into linear optical response calculations, aggressively raises the conduction states to higher energy while maintaining the number of electronic wavefunctions.

### 2.3.4 Optical response

Polarization induced by electromagnetic wave (EM) in linear optical material is directly proportional to the electric field.

$$\boldsymbol{P} = \varepsilon_o\chi\boldsymbol{E} \qquad \text{(Eq. 2.33)}$$

where $\chi$ is the linear susceptibility with the matching dielectric constant $\varepsilon = \varepsilon_o(1+\chi)$. When intensity of EM wave grows stronger, a shift from linear behavior to nonlinear pattern occurs. As a result, the dielectric constant becomes a field-dependent parameter [38, 39, 40, 41]. Expanded terms of susceptibility and related dielectric constant are as follows:

$$\chi(\boldsymbol{E}) = \chi + \chi^{(2)}\boldsymbol{E} + \chi^{(3)}\boldsymbol{E}^2 + \cdots \quad \text{(Eq. 2.34)}$$

$$\varepsilon(\boldsymbol{E}) = \varepsilon + \varepsilon^{(2)}\boldsymbol{E} + \varepsilon^{(3)}\boldsymbol{E}^2 + \cdots \quad \text{(Eq. 2.35)}$$

When combined

$$\boldsymbol{P} = \varepsilon_o\chi\boldsymbol{E} + \varepsilon_0\chi^{(2)}\boldsymbol{E}^2 + \varepsilon_o\chi^{(3)}\boldsymbol{E}^3 + \cdots = \boldsymbol{P}^{(1)} + \boldsymbol{P}^{(2)} + \boldsymbol{P}^{(3)} + \cdots \quad \text{(Eq. 2.36)}$$

in which

$$\boldsymbol{P}^{(1)} = \chi_{ab}\left(-\omega_\beta, \omega_\beta\right)e^{-i\omega_\beta t}\boldsymbol{E}^b\left(\omega_\beta\right) \quad \text{(Eq. 2.37)}$$

$$\boldsymbol{P}^{(2)} = \chi_{abc}\left(-\omega_\beta, -\omega_\gamma, \omega_\beta, \omega_\gamma\right)e^{-i(\omega_\beta+\omega_\gamma)t}\boldsymbol{E}^b\left(\omega_\beta\right)\boldsymbol{E}^c\left(\omega_\gamma\right) \quad \text{(Eq. 2.38)}$$

From perturbation approach, values of single particle operator $\Phi$ is expressible as

$$\Phi_\lambda = \lambda\Phi^{(1)} + \lambda^2\Phi^{(2)} + \lambda^3\Phi^{(3)} + \cdots \quad \text{(Eq. 2.39)}$$

where

$$\Phi^{(1)} = \sum_{nmk} f_{nm}(\boldsymbol{k})\Phi_{nm}(\boldsymbol{k}, t)\frac{\mu^b_{mn}(\boldsymbol{k}, t)}{\left(\omega_{mn} - \omega_\beta\right)} \times e^{-i\omega_\beta t}\boldsymbol{E}^b\left(\omega_\beta\right) \quad \text{(Eq. 2.40)}$$

$$\Phi^{(2)}$$

$$= i\sum_{nmk} f_{nm}(\boldsymbol{k})\Phi_{nm}(\boldsymbol{k}, t)\frac{1}{\left(\omega_{mn} - \omega_\beta - \omega_\gamma\right)}$$

$$\times \frac{\delta}{\delta z}\left[\frac{\mu^b_{mn}(\boldsymbol{k}, t)}{\omega_{mn}(z) - \omega_\beta}\right]e^{-i(\omega_\beta+\omega_\gamma)t}\boldsymbol{E}^b\left(\omega_\beta\right)\boldsymbol{E}^c\left(\omega_\gamma\right) \quad \text{(Eq. 2.41)}$$